# Ion Optics for High Power 50-cm-diam Ion Thrusters

Vincent K. Rawlin and Marc G. Millis
*Lewis Research Center*
*Cleveland, Ohio*

**NASA**

# ION OPTICS FOR HIGH POWER 50-cm-diam ION THRUSTERS

Vincent K. Rawlin and Marc G. Millis
National Aeronautics and Space Administration
Lewis Research Center
Cleveland, Ohio 44135

## ABSTRACT

Propulsion systems analyses have indicated that high power xenon ion thrusters can enable the use of smaller launch vehicles for orbit transfer missions and, thereby, result in major cost benefits. The 50-cm-diam thrusters, proposed to satisfy the mission requirements, have been fabricated and evaluated. Because the ion optics are considered to be the most critical component, they were subjected to extensive mechanical and electrical evaluation. The ion optics fabrication process, used at NASA Lewis Research Center for the past 18 years to make 30- and 50-cm-diam ion optics is described. The 50-cm-diam ion optics were vibration tested with no apparent damage. The ion extraction capabilities of 30- and 50-cm-diam ion optics were evaluated on divergent field and ring-cusp discharge chambers and compared. Sensitivities of perveance to discharge chamber type, discharge chamber power, and accelerator electrode hole diameters were observed. Thrust and input power levels up to 0.64 N and 20 kW, respectively, were demonstrated with the divergent field discharge chamber. Thruster efficiencies and specific impulse values up to 79 percent and 5000 sec were achieved with the ring-cusp discharge chamber.

## INTRODUCTION

Recent analyses have shown that ion propulsion upper stages for orbit transfer missions enable the use of smaller launch vehicles which can result in significant cost savings (refs. 1 and 2). In the interest of reducing propulsion system complexity, high power xenon ion thrusters were assumed in those studies. Experiments at the NASA Lewis Research Center with 10 kW class divergent field (ref. 3) and ring-cusp (ref. 4) 30-cm-diam xenon ion thrusters have shown a potential for reduced risk by operating a 50-cm-diam thruster at a derated thrust level. Therefore, larger 50-cm-diam thrusters were fabricated and initial test results describing their performance at this power level have been presented (ref. 5).

The ion extraction system, or ion optics, is considered to be the most critical ion thruster component because it typically processes more than 80 percent of the thruster input power. It also limits the maximum values of thrust and power densities, especially at values of specific impulse between 2000 and 5000 sec, which are near optimum for orbit transfer missions. Requirements of ion thrusters for high thrust and relatively low specific impulse imply increased ion extraction capability through larger area beams and minimum grid-to-grid spacings. This combination can lead to unprecedentedly large span-to-gap ratios of the ion optics.

Flat perforated plate electrodes, with a span-to-gap ratio of 60, evolved during the development of high specific impulse mercury ion thrusters for planetary space propulsion (ref. 6). When this technology was applied to larger

diameter, lower specific impulse engines, flat electrodes were found to warp severely under thermal loading even when held in tension or separated with interelectrode supports (refs. 7 and 8). Interelectrode supports provided reduced span-to-gap ratios for 30-cm-diam thrusters but were found to suffer from elevated charge exchange erosion rates (refs. 8 and 9). Insulated single electrode optics were also found to be unsuccessful (ref. 10). The single insulated electrode ion optics provided both poor performance, when operated in a vacuum facility with nonmetallic target, and limited lifetime for reasons explained in reference 10.

Eventually, thermally stable 30-cm-diam, dished, two grid ion optics were fabricated and found to provide superior performance at relatively close grid-to-grid spacings (ref. 11). The span-to-gap ratio had been increased to about 600. For nearly two decades dished ion optics, ranging in diameter from 8 to 38 cm have been the preferred design of many ion sources for space propulsion and ground based applications (refs. 12 to 18).

The basic techniques used to successfully construct 30-cm-diam ion optics at NASA Lewis were retained to fabricate 50-cm-diam ion optics. This paper describes the fabrication process and presents the results of mechanical and electrical evaluations of 50-cm-diam ion optics. The discharge chamber design and accelerator grid hole diameter were the major hardware variables.

## SYMBOLS

$A_O$    accelerator electrode open area, $m^2$

$d_A$    accelerator electrode hole diameter, mm

$d_S$    screen electrode hole diameter, mm

EV    beam ion production cost, W/A

$e$    electronic charge, $1.6 \times 10^{-19}$ C

$F_{OA}$    accelerator electrode open area fraction

$F_{OS}$    screen electrode open area fraction

$g$    acceleration of gravity, $9.81$ m/sec$^2$

$I_{sp}$    specific impulse

$J_B$    ion beam current, A

$K_c$    clausing conductance factor

$k$    Boltzmann's constant, $1.38 \times 10^{-23}$, JK$^{-1}$

$m$    xenon atom mass, $2.18 \times 10^{-25}$ kg

$\dot{m}_I$    ingested flow rate, eq. A.

| | |
|---|---|
| P | thruster input power, W |
| $P_F$ | vacuum facility pressure, Pa |
| T | thrust, N |
| $T_W$ | vacuum facility wall temperature, K |
| $t_A$ | accelerator electrode thickness, mm |
| $t_S$ | screen electrode thickness, mm |
| $V_D$ | discharge voltage, V |
| $V_N$ | net accelerating voltage, V, Potential of discharge chamber plasma with respect to the local ground |
| $\alpha$ | thrust correction factor due to multiply – charged ions |
| $\gamma$ | total thrust correction factor including effects due to multiply-charged ions and beam divergence. |
| $\varepsilon$ | screen electrode hole pattern reduction to compensate for electrode hole misalignment, percent |
| $\eta_D$ | discharge propellant efficiency, uncorrected for multiply charged ions |
| $\eta_P$ | total thruster propellant efficiency uncorrected for multiply charged ions |
| $\eta_T$ | overall thruster efficiency |

## APPARATUS AND PROCEDURE

### Ion Optics Fabrication

Figure 1 shows the steps of the NASA Lewis ion optics fabrication process. Fifteen years ago, 30-cm-diam ion optics were fabricated from low carbon arc cast molybdenum sheet. Since then, pressed and sintered molybdenum improved in quality and became available in a deep draw grade for high stress forming operations. The sintered molybdenum was selected for 50-cm-diam ion optics. Cross-rolling of this material was also specified. The flat molybdenum sheets were then sent to a vendor for application of both a photosensitive coating in the desired hole array pattern and indices to insure alignment. This coating was resistant to chemicals that etch molybdenum. The printed molybdenum sheets were returned to NASA Lewis where pairs of sheets were aligned and prepared for hydroforming.

The hydroforming apparatus of reference 11 was redesigned, as shown in figure 2, and has been used to fabricate all 30- and 50-cm-diam ion optics at NASA Lewis since those described in reference 11. Two flat molybdenum sheets, with photoresist patterns aligned, were placed between the upper and lower clamping rings, of the appropriate diameter, as shown in figure 2. A 0.38-mm

3

thick sheet of stainless steel was placed above the molybdenum pieces to reduce the stress on the molybdenum pieces at the locking "vee" groove. A piece of polyethylene was placed over each molybdenum sheet to protect the photoresist pattern from being scratched.

The pressure chamber plate and piston were then lowered onto the upper clamping ring and the lifting nuts lowered. Nuts were hand tightened onto the clamping bolts and the cavity above the piston was filled with water. A rubber sheet above the piston sealed the volume between the pressure chamber plate and the piston. An air-actuated hydrostatic pump pressurized the water in the cavity to $1 \times 10^7$ Pa (1500 psi), forcing the "vee" of the upper clamping ring and metal sheets into the matching groove in the lower clamping ring. The water pressure was then removed and the clamping nuts were retightened by hand. The water above the piston was repressurized to $1.7 \times 10^7$ Pa (2500 psi).

A ring of rubber sheet between the baseplate and the lower clamping ring sealed the lower hydroforming cavity. A second air-actuated hydrostatic pump pressurized the water-filled cavity between the baseplate and the ion optics and forced the electrodes upward into the free space between them and the piston. As shown in figure 2 the electrodes were dished without the aid of a forming die. Hydroforming pressures up to $2.3 \times 10^6$ Pa (330 psi) were required to produce dish depths to 5.1 cm in 50-cm-diam ion optics. The resultant dish depth was nearly linear with hydroforming pressure. The formed ion optics were then removed from the hydroforming apparatus and returned to the vendor to chemically etch the holes into the solid molybdenum sheets and then remove the photoresist coating.

With the exception of the three sets of electrodes evaluated in reference 11, none of the 30- or 50-cm-diam electrodes fabricated at NASA Lewis were stress relieved. It was found, in reference 19, that additional grid shaping could occur during the stress relieving process. Performance comparisons of 30-cm-diam electrodes which were and were not stress relieved, showed no advantages of either technique. Therefore, it was decided to forgo the stress relieving step for laboratory hardware fabricated at NASA Lewis. Reference 20 documents the evolution of a stress relieving procedure which has been used in the development of xenon ion thrusters (ref. 17).

Table I lists the geometric properties of the 30- and 50-cm-diam⋅dished ion optics used in this investigation. The NASA Lewis built 30-cm-diam electrodes were attached at their perimeter to 0.38 cm thick, flat molybdenum rings which were held apart by aluminum oxide insulators located upstream of the optics plane in a manner similar to that described in reference 11. To electrically evaluate 50-cm-diam ion optics, they were separated by a ring of synthetic mica and held in compression by large diameter, 0.38-cm-thick molybdenum rings.

The cold grid-to-grid spacings of 50-cm-diam ion optics were found to be nonuniform whether they were assembled or unassembled. In most cases the minimum gap at the ion optics edge was significantly less than the centerline spacing. There are several possible reasons for the gap nonuniformity. First, regions of differing springback after hydroforming may occur due to variations in material thickness of up to 10 percent. The large span to thickness ratio also increased the fragility of the ion optics, some of which suffered varying degrees of deformation during handling. Variations up to 40 percent in the

thickness of the mica spacer rings also contributed to the large variations in the grid-to-grid spacing. In addition, the undished perimeter flange was not always flat and normal to the thruster axis. Therefore, stresses were probably induced in the electrodes when they were clamped between the mounting rings. Such stresses may have led to changes in the grid-to-grid spacing under thermal loading of thruster operation.


## Ion Optics Mechanical Evaluation

Vibration and shock tests of individual 50-cm-diam electrodes and an assembly of electrodes were conducted at the Structural Dynamics Laboratory at NASA Lewis to evaluate their structural integrity. Table II lists the pertinent test parameters. All vibration table motion was vertical, along the axis of symmetry of the electrodes as shown in figure 3. Ion optics set 8, which is identical in aperture dimensions to state-of-the-art 30-cm-diam ion optics (ref. 13.), was vibrated. Set number 8 represents the expected geometric extremes for screen and accelerator electrode open area fractions of 0.67 and 0.24, respectively. In all cases, the single or double electrodes were clamped to the vibration table by a 1.27 cm thick, 13.2 cm wide aluminum ring which was cut into eight equal segments.

For all single electrode tests, the vibration table motion was controlled by the output of a single accelerometer located at the inner edge of the segmented clamping ring, which was adjacent to the dished region of the electrodes as shown in figure 3. For the two-electrode tests (runs 6 and 7) the feedback signal from another accelerometer, located 180° from the one used for runs 1 to 5, was averaged with the first signal to control the table motion. The individual electrodes were first tested for resonant frequencies with a sine sweep from 5 to 2000 Hz at an acceleration of 0.25 g and a sweep rate of 3 octaves per minute. The electrodes were then evaluated with random vibration at 4.2 and/or 15 g. The individual electrodes were then assembled with a 0.76-mm-thick mica ring and random vibration tested at 15 g and shock tested to a 36-g peak with three half-sine pulses of about 8 msec duration.

Three response accelerometers were used for each single electrode test. One accelerometer was attached to the center of the electrode and the other two were located at half-radius, 90° apart. No response accelerometers were used for the two-electrode assembly. Instead, a 1.5 V battery powered continuity checking circuit and event counter were used to monitor electrode contact during the 15 g random vibration test.


## Ion Optics Electrical Evaluation

The ability of a set of electrodes to efficiently extract an ion beam from a discharge chamber is measured by its "perveance." Perveance for a diode configuration is defined as the space charge limited current divided by the three-halves power of the potential difference between the electrodes. The perveance limited ion beam current is achieved when a significant increase in accelerator grid current is obtained, due to ion defocusing from space charge effects, as the total accelerating voltage is reduced. To provide margin, normal ion optics operation occurs at total voltages about 200 V or more above the minimum value, or at beam currents about 15 percent or more below the maximum value.

Deviations from the dependency on the three-halves power of the potential difference between the discharge plasma and the accelerator grid have been observed, and were usually greater than three-halves, (refs. 11 and 21). These deviations have been attributed to variations in the electrode spacing during operation, and to differences between actual ion thruster conditions and the assumptions made for the ideal planar diode. Some of these differences were discussed in detail in reference 22.

The ion extraction capabilities of 30-cm-diam ion optics sets 1, 2, and 3, evaluated on several 30-cm-diam discharge chambers, were compared. Optics set 3 was also evaluated on the 50-cm-diam ring-cusp discharge chamber to allow comparisons with 50-cm-diam optics sets 4 to 7 which were evaluated on the 50-cm-diam discharge chambers. Table I lists the different ion optics sets and identifies those discharge chamber-ion optics combinations evaluated.

## Discharge Chambers

The 30-cm-diam divergent field and ring-cusp discharge chambers designated "30DIV" and "30RC," respectively, were employed to evaluate 30-cm-diam ion optics sets 1, 2, and 3 in references 21, 3, and 4, respectively. The ion extraction capabilities of optics sets 3 to 7 were evaluated on at least one of the three 50-cm-diam discharge chamber configurations shown in figures 4 to 6. The main difference between the discharge chambers was that one, designated "50DIV" (fig. 4), utilized a weak divergent magnetic field generated throughout the chamber volume with electromagnets to contain the plasma while the other two (figs. 5 and 6) incorporated rings of rare-earth permanent magnets to produce strong boundary cusp magnetic fields. The ring-cusp geometry was designated "50RC." When optics set 3 was evaluated on 50RC, an adapter plate was required as shown in figure 6. This mild steel plate was electrically isolated from the discharge chamber and usually held at cathode potential. It had either 0 or 2 layers of magnet arranged in three rings. These two configurations were designated "50RC0" and "50RC2," respectively. Additional discharge chamber information has been presented in references 3 to 5 and 23.

## Vacuum Facilities

Ion optics evaluations were conducted in two large vacuum facilities at NASA Lewis. The divergent field thruster was operated in a 7.6-m diam by 21.3-m long vacuum facility while the ring-cusp thruster was operated in a 4.6-m diam by 19.2-m long facility. Vacuum facility pressures, without propellant flow, were about $1 \times 10^{-4}$ Pa ($8 \times 10^{-7}$ torr) and were achieved with twenty 0.8-m-diam oil diffusion pumps. During thruster operation, the facility pressure varied from 0.5 to $2 \times 10^{-3}$ Pa (0.4 to $1.6 \times 10^{-5}$ torr) for xenon flow rates of 3 to $12 \times 10^{-6}$ kg/s. At these pressures, non-negligible amounts of facility residual gas may be ingested by the thruster and contribute to the discharge chamber neutral density.

This flow rate was estimated from equation (1) (ref. 23) as:

$$\dot{m}_I = \frac{PFA_oK_ce}{\sqrt{2\pi mkT_w}} \text{ , eq. A.} \tag{1}$$

6

Symbols are defined in the SYMBOLS list.

## Power Supplies

Two similar 60 Hz laboratory power supply systems were used interchangeably to evaluate the ion optics. They have been described in references 3 and 21.

## Overall Thruster Performance

Values of input power, thrust, specific impulse, and efficiency were calculated using the equations and assumptions of reference 23.

## RESULTS

The structural integrity and ion extraction capability of 50-cm-diam ion optics were evaluated. Values of overall thruster performance using these optics were also calculated.

## Ion Optics Mechanical Evaluation

Resonant search. - Resonant searches of individual screen and accelerator electrodes (runs 1 and 4, table II) were conducted using a 0.25 g amplitude sine sweep. The response spectra of accelerometers located at the centers of the screen and accelerator electrodes are shown in figures 7(a) and (b), respectively. These spectra clearly show closely spaced higher order resonant frequencies above about 600 Hz for the screen electrode and 900 Hz for the accelerator electrode. Acceleration amplification factors at the center of each electrode were as high as 370 for the screen electrode and 140 for the accelerator electrode. The maximum acceleration levels obtained at the screen electrode half radius were 3200 and 270 percent lower than that at the screen electrode center. The maximum acceleration levels obtained at the accelerator electrode half radius were only 34 and 14 percent lower than that at the accelerator electrode center. The accelerator electrode is more massive than the screen electrode because it has a lower open area fraction. These large variations may be due to excitation of different mode shapes for each electrode. The absence of a clear consistent fundamental frequency and subsequent harmonics, for the electrodes during sine and random vibration tests, indicates the complexity of the problem. For example, the low frequency "resonance" at 150 Hz (fig. 7(a)) was observed only during run 1 of the screen electrode and is not understood at this time.

For purposes of comparison, an accelerometer, located at the center of the accelerator electrode of a complete 30-cm-diam mercury ion thruster, indicated resonant frequencies from 135 to 270 Hz during a sinusoidal vibration test with an 11 g input. Amplification factors at these frequencies of about 10 were measured (ref. 24). Electrode shape, dimensions, and mounting techniques would be expected to significantly impact the responses.

7

Random vibration. - The 4.2 g random vibration input spectrum (run 2), shown in figure 8(a), was selected to be representative of a Titan III launch vehicle. The desired random vibration spectrum was specified and boundaries, ±3 dB from the desired acceleration spectral density, were drawn. The vibration table motion was controlled to provide acceleration spectral density values within these boundaries. The peak and total integrated responses of the accelerometer located at the center of the screen electrode were 624 and 111 g, respectively, and were obtained from the spectrum shown in figure 8(b). The total integrated response is defined as the square root of the area under the spectrum. As it was for the sine sweep, the response was negligible up to 600 Hz and the maximum acceleration occurred at about 1300 Hz. At 1300 Hz, the peak acceleration amplification factor was about 310. At this frequency both the maximum acceleration and total integrated response acceleration, indicated by the two half-radius accelerometers, were 1.7 and 2.7 times less than that at the center. The order of the half radius results given here is the same as that given for the sine sweep. Note that the relative responses of the sine and random runs are very different.

Because there was no apparent physical damage to the screen electrode, the vibration table input level was raised to 15 g (run 3) with the spectrum shown in figure 9(a). The response spectrum for the center of the screen electrode is shown in figure 9(b). The peak and total responses were about 1140 and 320 g, respectively, with the amplification factor at the peak acceleration dropping to about 180. At half-radius, the spectra peaks near 600 Hz, for both accelerometers were greater than those near 1300 Hz with amplification factors ranging from 40 to 110. Again, there was no apparent damage.

The accelerator electrode was vibrated in a random motion with only a 15 g input level (run 5) having boundary levels identical to those of figure 9(a). The response of the center accelerometer is shown in figure 9(c). Peak values of acceleration, of about 670 g, were observed at frequencies near 1000 and 1500 Hz giving acceleration amplification factors of 70 and 100, respectively. The total integrated response was 211 g. Assembled as a set, with a spacing of about 0.76 mm, the screen and accelerator electrodes were subjected to a random vibration test (run 6) at 15 g. The input spectrum boundaries were the same as in figure 9(a). Displacements of the assembled electrodes were sufficient to cause repeated electrode contact throughout the run. Based on this fact and a simplified analysis, the centerline electrode displacements at the resonant frequencies were estimated to be about 0.5 mm. However, after the run, inspection indicated, as in the cases of single electrodes, that no damage had occurred.

In summary, the energies in the response spectra were concentrated in the higher order resonant frequency domains, as expected, although the main energy contents of the random input spectra were in the frequency range below 800 Hz. Due to acceleration amplification factors of several hundred times the inputs at the resonant frequencies, the high frequencies involved led to displacements of order 0.5 mm which caused electrode contact. These displacements apparently had little potential for damage during either sine or random vibration testing.

Shock test. - A series of three half-sine 36.4-g shock pulses were conducted during run 7 to conclude this preliminary structural testing. The specimens showed no visible evidence of damage when inspected at the conclusion of the test sequence.

## Ion Optics Electrical Evaluation

The ion extraction capabilities, of ion optics sets 3 to 7 from table I, were evaluated on the 50-cm-diam discharge chambers, as shown in table I, and compared.

The 30-cm diam ion optics. - Figure 10 compares the xenon ion extraction capabilities of three sets of 30-cm-diam ion optics which were identical, except that the accelerator grid hole diameters of optics set 3 were 11 percent greater than those of set 1 and the accelerator grid thicknesses of optics sets 2 and 3 were 33 percent greater than that of set 1. The ion optics were evaluated on four different discharge chamber configurations. The circular and square data points, obtained with optics sets 1 and 3, respectively, evaluated on identical, modified J-Series discharge chambers described in references 21 and 3, respectively, define nearly identical ion extraction capabilities.

Figure 10 also shows the ion extraction capability of optics set 2 evaluated on the NASA Lewis baseline 30-cm-diam ring-cusp discharge chamber (ref. 4). Compared to optics sets 1 and 3 on the divergent field discharge chamber, the perveance of optics set 2 is between 30 and 40 percent lower than that of optics set 3. Applying the sensitivities of perveance to changes in accelerator grid hole diameter (ref. 24) and cold grid spacing (ref. 22) to the geometric differences between optics sets 2 and 3, their perveances should have been identical if evaluated on the same discharge chamber. One possible explanation for the perveance difference, offered in reference 5, was that ring-cusp thrusters typically exhibit current density profiles which are more axially-peaked than those of divergent field thrusters. Beam current density profiles were not measured for any of the data of figure 10. The perveance difference was not due to differences in discharge power (and, thereby, unlikely to be due to thermal differences) because the ion production costs (discharge watts per beam ampere), for values of beam current 2A and above, were constant within 10 percent for both sets of data.

When ion optics set 3 was evaluated on the 50-cm-diam ring-cusp discharge chamber, the adapter plate had either no magnets (50RC0), or three rings of double-layer magnets (50RC2) to reduce the ion wall losses (refs. 5 and 23). Compared to the J-Series discharge chamber, the ion extraction capability for 50RC0 was about 20 percent greater and that of 50RC2 about 20 percent below. With magnets on the adapter plate, the discharge power of 580 W (discharge voltage times emission current) required to produce a beam current of 2.3 A was half that when no magnets were used. Thus, the ion optics were probably hotter for the case without adapter plate magnets which may have resulted in a closer grid-to-grid spacing and higher perveance. The presence of strong field magnets near the ion optics may have also altered the plasma density profile. Compared to the ion extraction capability of the NASA Lewis baseline 30-cm-diam ring-cusp thruster, the ion extraction capabilities for 50RC0 and 50RC2 were about 80 and 40 percent greater.

The 50-cm-diam ion optics; divergent field thruster. - The ion extraction capabilities of 50-cm-diam optics evaluated on the 50-cm-diam divergent field discharge chamber are shown in figure 11. The solid lines are boundaries for scatter in the data. There are several notable features which will be discussed separately for each optics set.

9

The perveance data for ion optics set 4 contain variations of nearly 50 percent which appeared to be primarily a function of discharge power. For example, the data points connected by nearly vertical dashed lines were obtained at thermal equilibrium conditions and constant propellant flow rates with only variations in discharge power (primarily discharge current) and consequently, propellant efficiency. However, when the discharge power was held nearly constant at values between 500 and 550 W the resulting perveance was also constant. The space charge limited beam current increased from 1.7 to 3 A with the three-halves power of the total accelerating voltage and only increases of propellant flow rate as indicated by the solid line connecting the six circular data points at 3 A or less. Values of propellant efficiency for these points, ranged from about 0.4 to 0.5. The maximum values of propellant efficiency for optics set 4 were limited by the high open area fraction of the accelerator electrode which allowed significant losses of neutral propellant. Similarly, the four optics set 4 data points connected by the upper solid line, were obtained as the discharge power and propellant efficiency were increased, respectively, from only 870 to 1130 W and from 0.6 to 0.7. Assuming thermal radiation was the dominant heat loss mechanism, this power change would be expected to raise the average electrode temperature only about 7 percent and have a negligible effect on perveance. Again, the perveance was nearly constant. Thus, it appears that part of the observed increases in perveance, with increases in beam current and discharge power, which are reflected as a greater than three-halves dependency may be due to electrode temperature increases which can lead to electrode spacing decreases. Possible variations in plasma density profile may also contribute to the perveance variations.

The thermal response time of the molybdenum electrodes is very short, whereas that of the molybdenum mounting ring adjacent to the screen electrode was found to be about 2 hr for a discharge power input change from 0 to 850 W. Therefore, only perveance data obtained 2 hr after start-up were presented. When taken during the warm-up period, perveance data were below the lower solid lines for each ion optics geometry and not repeatable. The ion extraction capabilities of ion optics sets 5 and 6, which had smaller accelerator electrode holes, were less than that of set 4. This trend was anticipated, based on results with 30-cm optics presented in reference 25, but the sensitivity was greater than expected. As with ion optics set 4, variations in the perveance with discharge power were large (up to 35 percent). Again, the points connected by dashed lines were obtained at constant propellant flow rates with only discharge power varied.

When ion optics set 7 was evaluated, the perveance was so low only limited data were obtained. During evaluation of ion optics set 5, the accelerator electrode impingement current initially dropped from 17 percent of the beam current, to less than 2 percent after 6 hr. Post test inspection revealed that ion beamlets were striking the walls of the accelerator electrode holes, especially at the outer radii. This erosion was not circumferentially symmetric, which indicated localized regions of misalignment and/or large grid spacing variations during operation. The best perveance of optics set 7 was less than that of optics set 3 (which had nearly the same geometry) even though the ion extraction area was nearly triple that of optics set 3.

For 30-cm-diam ion optics evaluated at a beam current of 2 A on a 30-cm-diam, divergent field mercury ion thruster, the minimum total accelerating

voltage increased from about 1050 to 1190 V as the accelerator grid hole diameter was decreased from 1.91 to 1.14 mm. Considering lighter xenon propellant and larger area 50-cm-diam ion optics, beam currents of 7.5 A were expected for the same total voltage and accelerator hole diameter ranges as used with 30-cm-diam configurations. Figure 11 shows that beam current extrapolations to these conditions varied, at best, from 5.6 A for optics set 4 to only about 1.2 A for optics set 7. Thus, not only were the levels of beam current lower than expected, but, they were more sensitive to variations in accelerator hole diameter than for 30-cm-diam ion optics. The sensitivity of impingement-limited normalized perveance per hole to accelerator grid hole diameter observed in reference 26 for small area optics was nearly identical to that observed for 50-cm-diam optics. The causes of the behavioral differences between 30- and 50-cm-diam ion optics are not known at this time. However, it is known that the fabrication quality of these first generation 50-cm-diam ion optics is poor and that the edge spacing variations are large compared to those of 30-cm-diam ion optics.

The 50-cm-diam ion optics, ring-cusp thruster. - The ion extraction capabilities of the 50-cm-diam optics were also evaluated with the 50-cm-diam ring-cusp discharge chamber, as shown in figure 12.

The sensitivity of optics perveance to discharge power and resultant thermal effects, shown in figure 11, was not observed with the ring-cusp discharge chamber. This result may be attributed to the fact that the ring-cusp discharge chamber produces ions more efficiently than the divergent field geometry and would be expected to have reduced thermally related effects on the ion optics.

Reference 23 showed that for propellant efficiencies in excess of 0.8, the ion production costs for the ring-cusp thruster decreased from about 170 to 100 W per beam ampere with decreasing accelerator electrode hole diameter (optics sets 4, 6, and 7). For the data of figure 12, typical ion production costs, for propellant efficiencies of 0.7 and above, were typically 40 to 70 percent less than those of the divergent field discharge chamber (fig. 11). In addition to differences in the levels of discharge power, differences exist, between each discharge chamber design, in the distribution of that power. The electron current in divergent field thrusters is collected at the downstream end of the anode (ref. 27), while it is more uniformly distributed in ring-cusp thrusters (ref. 19). These variations would be expected to result in lower steady-state temperatures of the electrodes and mounting rings when tested on the ring-cusp thruster and are probably the major causes of the differences in response to changes in discharge power. These effects may produce smaller changes in the electrode gap at thermal equilibrium which would result in lower perveance values than those obtained with the divergent field discharge chamber.

The sensitivity of perveance to accelerator electrode hole diameter was nearly the same as that found with the divergent field discharge chamber. However, the perveance of each optics set evaluated on the ring-cusp discharge chamber was always lower than it was for the divergent field geometry. The differences were about 30 percent for optics sets 4, 5, and 6 and about 20 percent for set 7. The differences are believed to be primarily due to variations in the thermal environments and/or plasma density distributions as explained

earlier. Thus, the improved performance of the ring-cusp discharge chamber was offset slightly by a reduction in the ion extraction capability.

This penalty was minor relative to the reduced levels of beam current obtained compared with those anticipated based on the performance of 30-cm-diam ion optics. Fabrication process improvements, such as stress relieving, may reduce grid spacing variations and hole misalignment.

## Overall Thruster Performance

Values of overall thruster performance were calculated for both 50-cm-diam discharge chambers operated with 50-cm-diam ion optics using demonstrated conditions. Tables III and IV list the operating conditions and calculated performance values for the 50-cm-diam divergent field and ring-cusp xenon ion thrusters. Figures 13 and 14 present the thrust obtained as a function of thruster input power and thruster efficiency as a function of specific impulse, respectively. Figure 13 shows that the thrust increased nearly linearly from 0.09 to 0.64 N as the thruster input power was raised to 20 kW. Thrust-to-power ratios varied from 41 to 32 mN/kW for the data shown. Figure 14 shows that thruster efficiency increased nearly linearly from 34 to 79 percent as the specific impulse was raised from 1700 to 5000 sec and was relatively insensitive to ion optics geometry or discharge chamber type. Therefore, over this range the thrust-to-power ratio would be expected to be nearly constant as observed in figure 13. Because ion thruster efficiency is essentially determined by specific impulse, the selection of a given geometry is not based on performance but on other factors, such as lifetime.

A divergent field 30-cm-diam xenon ion thruster, operated for 567 hr at 10 kW, experienced intolerable erosion rates of the discharge baffle (ref. 3). Reference 5 showed severe performance degradation with the baffle removed. However, the ring-cusp geometry yields superior performance without the need for a discharge baffle (refs. 5 and 19). Therefore, thrusters incorporating the ring-cusp magnetic field design are now the baseline geometry (refs. 4 and 23).

## CONCLUSIONS

Interest in high power, high specific impulse xenon ion thrusters is increasing. Thrusters with diameters greater than 30 cm offer prospects for improved lifetime and a more modest thermal environment. Therefore, 50-cm-diam ion thrusters have been evaluated at NASA Lewis. Because they typically process more than 80 percent of the thruster input power, the ion optics are considered to be the most critical component of ion thrusters.

The fabrication process and apparatus used at NASA Lewis to construct 30- and 50-cm-diam ion optics were described. Stress relieving the electrodes after hydroforming had been omitted from the NASA Lewis process without deleterious effects on 30-cm-diam optics but may be required for larger electrodes.

The 50-cm-diam ion optics with screen and accelerator electrode open area fractions of 0.67 and 0.24, respectively, were vibrated to levels several times

those representative of the Titan III launch vehicle and subjected to repeated 36 g shocks. No damage was observed for electrodes vibrated singly or as a set.

The ion extraction capabilities of state-of-the-art 30-cm-diam ion optics were evaluated on a 50-cm-diam ring-cusp discharge chamber and found to be as much as 20 and 80 percent greater than those obtained when evaluated on 30-cm-diam divergent field and ring-cusp discharge chambers, respectively.

The ion extraction capabilities of four sets of 50-cm-diam optics were evaluated on 50-cm-diam divergent field and ring-cusp discharge chambers. The general perveance level was significantly less than expected based on the ion extraction capabilities of 30-cm-diam optics. In addition, the sensitivity of perveance to accelerator electrode hole diameter was stronger for 50-cm-diam optics than for 30-cm-diam optics. A sensitivity of 50-cm-diam ion optics perveance to discharge power level was observed with the divergent field discharge chamber but not with the more efficient ring-cusp geometry. In addition, the perveance of a given set of ion optics was 20 to 30 percent lower on the ring-cusp discharge chamber compared to that obtained with the divergent field geometry. These effects may be thermally induced and, therefore, sensitive to discharge power and temperature distributions.

Values of overall thruster performance were calculated from demonstrated discharge chamber and ion optics conditions. The thrust increased from 0.09 to 0.64 N as the thruster power was increased to 20kW and thruster efficiency increased from 34 to 79 percent as the specific impulse was increased from 1700 to 5000 sec. These performance values were relatively insensitive to ion optics geometry or discharge chamber type. Therefore, selection of the ring-cusp thruster design was based on other factors, such as lifetime.

As the ion optics fabrication procedure and mounting design mature, 50-cm-diam ion thrusters should have a significant potential for growth in thrust and power levels.

## REFERENCES

1. Deininger, W.D. and Vondra, R.J., "Electric Propulsion for Constellation Deployment and Spacecraft Maneuvering," AIAA Paper 88-2833, July 1988.

2. Sponable, J.M. and Penn, J.P., "Electric Propulsion for Orbit Transfer - A Navstar Case Study (Has Electric Propulsion's Time Come?)," AIAA Paper 87-0985, May 1987.

3. Rawlin, V.K., "Internal Erosion Rates of a 10-kW Xenon Ion Thruster," AIAA Paper 88-2912, July 1988 (NASA TM-100954).

4. Patterson, M.J. and Curran, F.M., "Electric Propulsion Options for 10-kW Class Earth-Space Missions," presented at 1989 JANNAF Propulsion Meeting, Cleveland, OH, May 23-25, 1989.

5. Patterson, M.J. and Rawlin, V.K., "Performance of 10-kW Class Xenon Ion Thrusters," AIAA Paper 88-2914, July 1988 (NASA TM-10292).

6. Kerslake, W.R., Goldman, R.G., and Nieberding, W.C., "SERT II: Mission, Thruster Performance, and In-Flight Thrust Measurements," Journal of Spacecraft and Rockets, Vol. 8, No. 3, Mar. 1971, pp. 213-224.

7. Bechtel, R.T., "Performance and Control of a 30-Centimeter Diameter, Low Impulse Kaufman Thruster", AIAA Paper 69-238, Mar. 1969.

8. King, H.J., et al., "Low Voltage 30 cm Ion Thruster," (NASA CR-120919) 1972.

9. Byers, D.C., "A Preliminary Investigation of Charge-Exchange Erosion of Accelerator Grid Supports," NASA TM X-67842, 1971.

10. Bechtel, R.T., Banks, B.A., and Reynolds, T.W., "Effect of Facility Back-sputtered Material on Performance of Glass-Coated Accelerator Grids for Kaufman Thrusters," AIAA Paper 71-156, Jan. 1971 (NASA TM X-52927).

11. Rawlin, V.K., Banks, B.A., and Byers, D.C., "Dished Accelerator Grids on a 30-cm Ion Thruster," Journal of Spacecraft and Rockets, Vol. 10, No. 1, Jan. 1973, pp. 29-35.

12. Power, J.L., "Planned Flight Test of a Mercury Ion Auxiliary Propulsion System. I - Objectives, Systems Descriptions, and Mission Operations," AIAA Paper 78-647-I, Apr. 1978 (NASA TM-78859).

13. Schnelker, D.E., Collett, C.R., Kami, S., and Poeschel, R.L., "Characteristics of the LeRC/Hughes J-Series 30-cm Engineering Model Thruster," AIAA Paper 79-2077, Oct. 1979.

14. Yamagiwa, Y., et al., "A 30-cm Diameter Xenon Ion Thruster - Design and Initial Test Results," IEPC Paper 88-095, Oct. 1988.

15. Groh, K.H., et al., "Inert Gas Performance of the RIT 35 Main Propulsion Unit," IEPC Paper 88-098, Oct. 1988.

16. Salazar, R.P., et al., "A Small Solar Electric Ion Propulsion Spacecraft for Lunar Science," AIAA Paper 88-2836, July 1988.

17. Beattie, J.R., Matossian, J.N., and Robson, R. R., "Status of Xenon Ion Propulsion Technology," AIAA Paper 87-1003, May 1987.

18. Kaufman, H.R., et al., "38-Centimeter Ion Source," Nuclear Instruments and Methods in Physics Research B, Vol. 37/38, Feb. 1989, pp. 98-102.

19. Poeschel, R.L., "Development of Advanced Inert-Gas Ion Thrusters," (NASA CR-168206) 1983.

20. Beattie, J.R. and Matossian, J.N., "Mercury Ion Thruster Technology," (NASA CR-174974) 1989.

21. Rawlin, V.K., "Operation of the J-Series Thruster Using Inert Gas," AIAA Paper 82-1929, Nov. 1982 (NASA TM-82977).

22. Rawlin, V.K., "Studies of Dished Accelerator Grids for 30-cm Ion Thrusters," AIAA Paper 73-1086, Oct. 1973 (NASA TM X-71420).

23. Rawlin, V.K., "Performance of Large Area Xenon Ion Thrusters for Orbit Transfer Missions," NASA TM-102049, 1989.

24. King, H.J., et al., "Low Voltage 30-cm Ion Thruster Development," (NASA CR-134731) 1974.

25. Rawlin, V.K., "Sensitivity of 30cm Mercury Bombardment Ion Thruster Characteristics to Accelerator Grid Design," AIAA Paper 78-668, Apr. 1978 (NASA TM-78861).

26. Rovang, D.C. and Wilbur, P.J., "Ion Extraction Capabilities of Two-Grid Accelerator Systems," NASA CR-174621, 1984.

27. Mirtich, M.J., "Thermal Environment Testing of a 30-cm Engineering Model Thruster," AIAA Paper 76-1034, Nov. 1976 (NASA TM X-73522).

TABLE I. – ION OPTICS GEOMETRY AND EVALUATION ENVIRONMENT

| Ion optics set | Fabricator | Diameter of ion extraction area, cm | $\varepsilon$,[a] per-cent | Dimensions | | | | | | | | Discharge chambers evaluated on |
|---|---|---|---|---|---|---|---|---|---|---|---|---|
| | | | | Screen electrode | | | Accelerator electrode | | | Cold spacing | | |
| | | | | $t_S$, mm | $d_S$, mm | $f_{OS}$ | $t_A$, mm | $d_A$, mm | $f_{OA}$ | Center, mm | Edge, mm | |
| 1 | Hughes Res. Lab | 28.7 | 0.35 | 0.38 | 1.91 | 0.67 | 0.38 | 1.14 | 0.24 | 0.50 | 0.50 | 30 DIV[b] |
| 2 | NASA Lewis | 28.7 | .30 | .38 | 1.91 | .67 | .51 | 1.14 | .24 | .66 | .66 | 30 RC[c] |
| 3 | | 28.7 | .30 | | | | .51 | 1.27 | .30 | .76 | .55 | 30 DIV, 50 RC0, 50 RC2 |
| 4 | | 49 | .20 | | | | .38 | 1.91 | .67 | .81 | .66 to 1.0 | 50 DIV, 50 RC |
| 5 | | | | | | | | 1.52 | .43 | 1.12 | .71 to 1.02 | 50 DIV |
| | | | | | | | | | | .86 | .30 to .66 | 50 RC |
| 6 | | | | | | | | 1.52 | .43 | .76 | .56 to 1.0 | 50 DIV, 50 RC |
| 7 | | | | | | | | 1.14 | .24 | .66 | .38 to .66 | 50 DIV, 50 RC |
| 8 | | | | | | | | 1.14 | .24 | 1.0 | .76 | Vibration table |

[a] Screen hole pattern reduction to compensate for electrode hole misalignment.
[b] DIV – Divergent magnetic field thruster.
[c] RC – Ring-cusp magnetic field thruster.

TABLE II. – 50-cm-diam ELECTRODE VIBRATION TEST PARAMETERS

| Run | Electrode | Vibration mode | Input acceleration level | Frequency range, Hz | Duration |
|---|---|---|---|---|---|
| 1 | Screen | Sine sweep | 0.25 g | 5 to 2000 | 3 oct/min |
| 2 | Screen | Random | 4.2 grms | 20 to 2000 | 1 min |
| 3 | Screen | Random | 15 grms | 20 to 2000 | 1 min |
| 4 | Accelerator | Sine sweep | 0.25 g | 5 to 2000 | 3 oct/min |
| 5 | Accelerator | Random | 15 grms | 20 to 2000 | 1 min |
| 6 | Assembly | Random | 15 grms | 20 to 2000 | 1 min |
| 7 | Assembly | Shock | 36.4 g | 3 half sine pulses | 7.7 ms each |

#### TABLE III. – OVERALL 50-cm-diam DIVERGENT FIELD XENON ION THRUSTER PERFORMANCE

| Ion optics set | $J_B$, A | $V_N$, V | $V_D$, V | EV, W/A | $\eta_D$ | $\eta_p$ | $\alpha$ | $\gamma$ | P, W | T, N | $I_{sp}$, s | $\eta_T$ |
|---|---|---|---|---|---|---|---|---|---|---|---|---|
| 4 | 2.3 | 600 | 30.6 | 289 | 0.590 | 0.569 | 0.998 | 0.978 | 2 240 | 0.091 | 1690 | 0.336 |
|   | 3.4 | 700 | 32.7 | 265 | .621 | .598 | .997 | .977 | 3 480 | .145 | 1910 | .390 |
|   | 4.2 | 820 | 32.6 | 253 | .658 | .633 | .997 | .977 | 4 700 | .194 | 2190 | .443 |
|   | 5.6 | 1100 | 32.7 | 230 | .752 | .729 | .995 | .975 | 7 650 | .299 | 2920 | .559 |
|   | 6.5 | 1400 | 33.0 | 221 | .800 | .762 | .993 | .973 | 10 700 | .390 | 3430 | .613 |
|   | 8.0 | 1500 | 32.0 | 228 | .720 | .691 | .995 | .975 | 14 000 | .498 | 3230 | .563 |
| 5 | 2.6 | 950 | 32.0 | 216 | .773 | .739 | .994 | .974 | 3 230 | .129 | 2750 | .538 |
|   | 3.8 | 1150 | 32.6 | 262 | .882 | .837 | .989 | .969 | 5 750 | .206 | 3410 | .618 |
|   | 5.4 | 1360 | 31.6 | 202 | .832 | .792 | .992 | .972 | 8 630 | .319 | 3510 | .636 |
|   | 6.2 | 1500 | 34.0 | 224 | .951 | .906 | .983 | .963 | 10 900 | .382 | 4180 | .718 |
| 6 | 4.2 | 1150 | 29.5 | 160 | .690 | .663 | .996 | .976 | 5 700 | .229 | 2720 | .535 |
|   | 6.2 | 1700 | 29.2 | 163 | .818 | .780 | .993 | .973 | 11 800 | .410 | 3870 | .659 |
|   | 7.3 | 1900 | 31.7 | 159 | .754 | .721 | .995 | .975 | 15 200 | .512 | 3790 | .626 |
|   | 8.8 | 2100 | 31.7 | 175 | .902 | .856 | .988 | .968 | 20 200 | .644 | 4700 | .734 |
| 7 | 2.6 | 1510 | 27.1 | 181 | .791 | .755 | .993 | .973 | 4 600 | .162 | 3530 | .609 |
|   | 4.1 | 1520 | 28.3 | 166 | .890 | .845 | .989 | .969 | 7 080 | .254 | 3950 | .694 |

#### TABLE IV. – OVERALL 50-cm-diam RING-CUSP XENON ION THRUSTER PERFORMANCE (ref. 23)

| Ion optics set | $J_B$, A | $V_N$, V | $V_D$, V | EV, W/A | $\eta_D$ | $\eta_p$ | $\alpha$ | $\gamma$ | P, W | T, N | $I_{sp}$, s | $\eta_T$ |
|---|---|---|---|---|---|---|---|---|---|---|---|---|
| 4 | 2.37 | 803 | 30.9 | 143 | 0.654 | 0.629 | 0.997 | 0.977 | 2 440 | 0.108 | 2160 | 0.468 |
|   | 3.16 | 830 | 31.0 | 165 | .875 | .831 | .990 | .970 | 3 340 | .146 | 2870 | .615 |
|   | 3.63 | 1300 | 32.0 | 165 | 1.01 | .948 | .975 | .956 | 5 520 | .206 | 4050 | .741 |
|   | 4.58 | 1300 | 29.5 | 131 | .839 | .799 | .992 | .972 | 6 750 | .265 | 3470 | .668 |
| 6 | 1.92 | 1030 | 32.0 | 151 | .840 | .800 | .992 | .972 | 2 470 | .099 | 3090 | .607 |
|   | 3.15 | 1440 | 32.2 | 133 | .909 | .862 | .987 | .967 | 5 150 | .191 | 3920 | .712 |
|   | 3.80 | 1800 | 30.2 | 164 | 1.09 | 1.02 | .953 | .934 | 7 660 | .248 | 5000 | .793 |
|   | 5.00 | 2000 | 25 | 136 | .807 | .770 | .993 | .973 | 10 900 | .359 | 4150 | .670 |
|   | 5.96 | 2100 | 29 | 129 | .965 | .912 | .981 | .961 | 13 500 | .433 | 4970 | .781 |
|   | 6.46 | 2200 | 24 | 126 | .788 | .752 | .994 | .974 | 15 200 | .487 | 4250 | .667 |
| 7 | 2.09 | 1535 | 31 | 109 | .499 | .484 | .999 | .980 | 3 640 | .132 | 2300 | .409 |
|   | 3.50 | 2080 | 30.3 | 101 | .836 | .800 | .992 | .972 | 7 830 | .256 | 4390 | .703 |
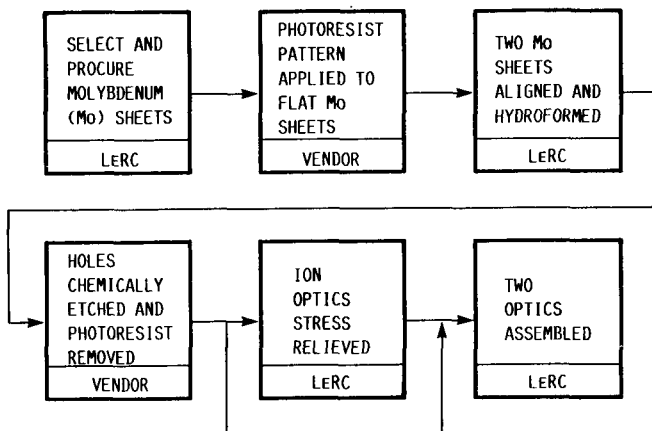


FIGURE 1. – ION OPTICS FABRICATION PROCEDURE.
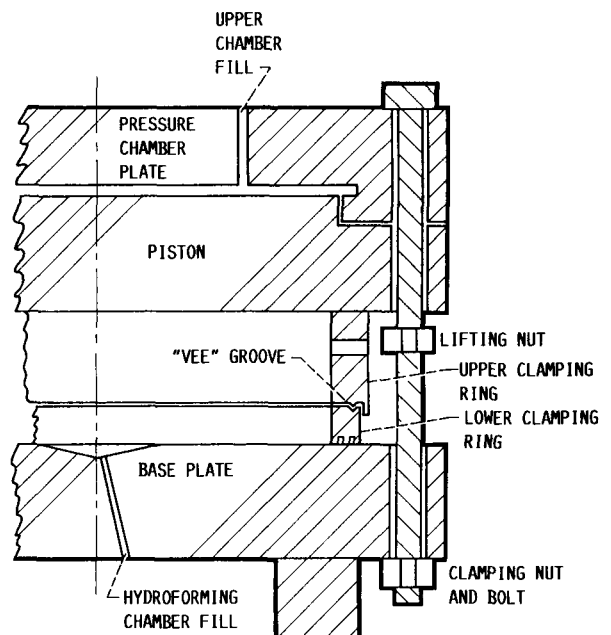


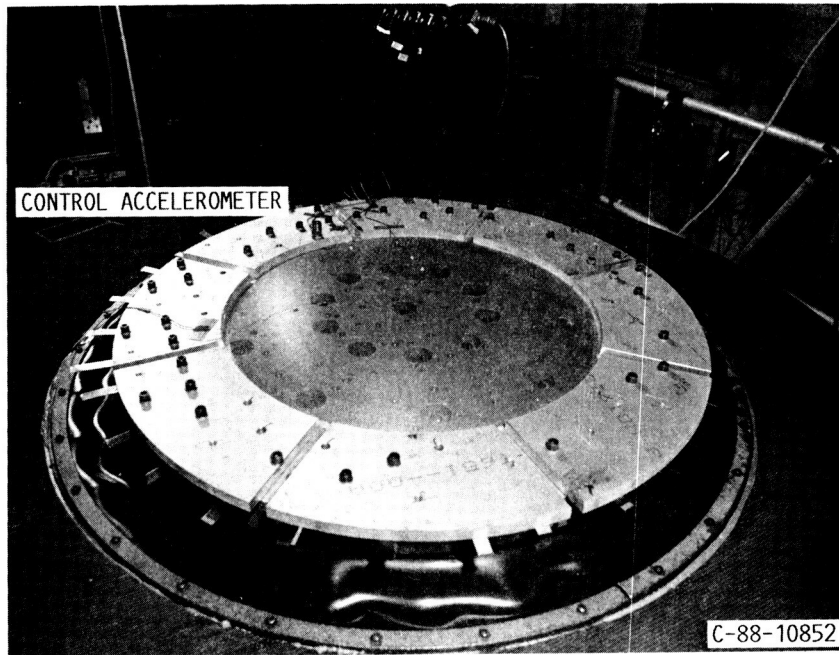FIGURE 2. – SECTION VIEW OF HYDROFORMING APPARATUS.

CONTROL ACCELEROMETER

C-88-10852

FIGURE 3. – 50-CM-DIAM SCREEN ELECTRODE CLAMPED TO VIBRATION
TABLE.



BAFFLE

HOLLOW CATHODE

FIELD LINE 70 G

~24.9 CM

ELECTROMAGNETS

ION OPTICS MOUNTING PLANE

ANODE

~14.9 CM
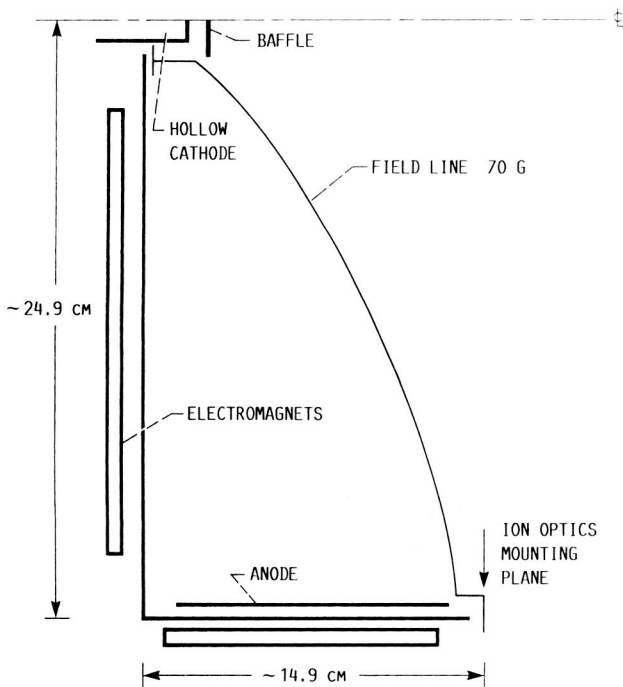
FIGURE 4. – 50-CM-DIAM DIVERGENT MAGNETIC FIELD DISCHARGE
CHAMBER (50 DIV.).



HOLLOW CATHODE

3600 G

SmCo MAGNETS

25.4 CM

ANODE

4600 G

ION OPTICS MOUNTING PLANE

3600 G

N  S  N  S  N

27.6 CM
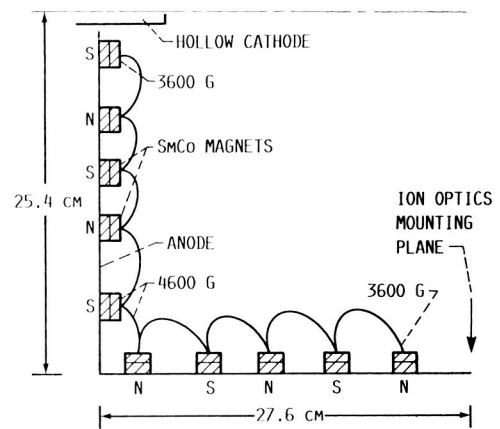
FIGURE 5. – 50-CM-DIAM RING-CUSP MAGNETIC FIELD
DISCHARGE CHAMBER USED WITH 50-CM-DIAM ION
OPTICS (50 RC).
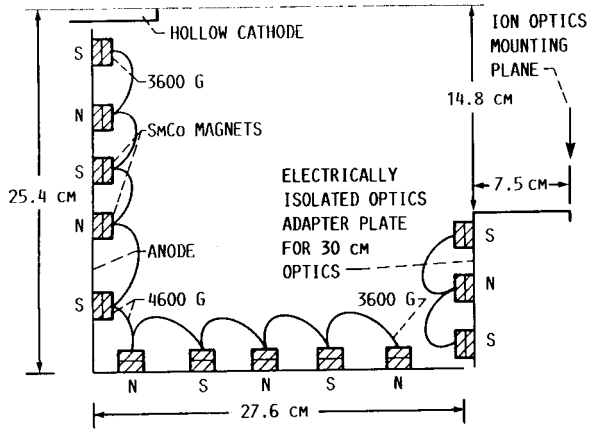
FIGURE 6. - 50-CM-DIAM RING-CUSP DISCHARGE CHAMBER USED WITH
30-CM-DIAM ION OPTICS (50 RC0, 50 RC2).



(A) SCREEN ELECTRODE (RUN 1).

(B) ACCELERATOR ELECTRODE (RUN 4).
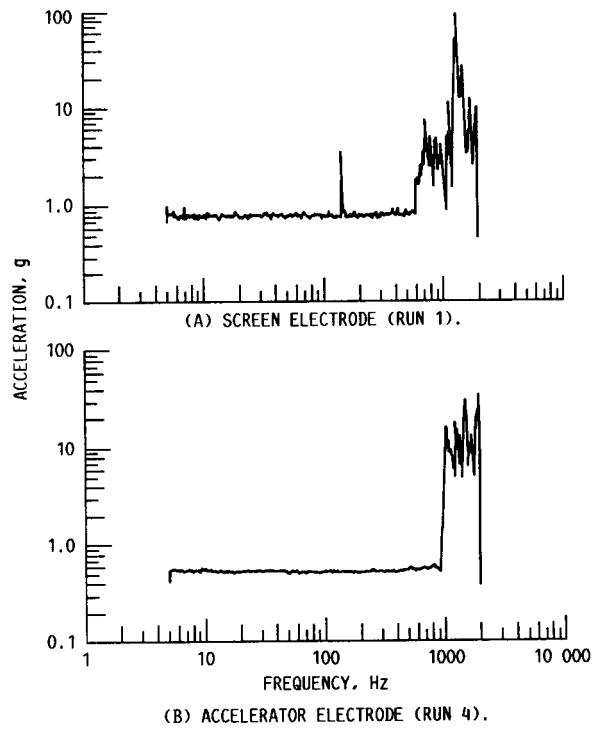
FIGURE 7. - RESPONSES OF ELECTRODE CENTER ACCELERO-
METERS TO 0.25 g SINE INPUT.
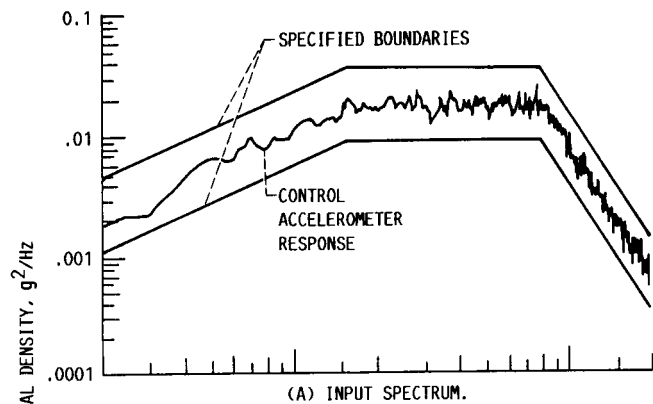


(A) INPUT SPECTRUM.
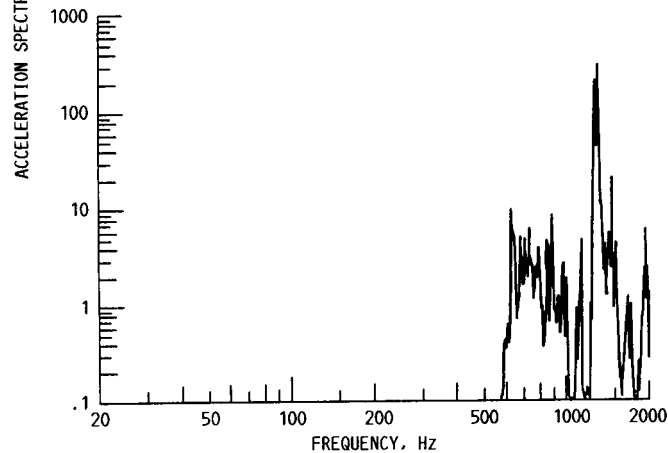
(B) RESPONSE OF SCREEN ELECTRODE CENTER ACCELEROMETER.

FIGURE 8. - RANDOM VIBRATION, REPRESENTATIVE OF TITAN III
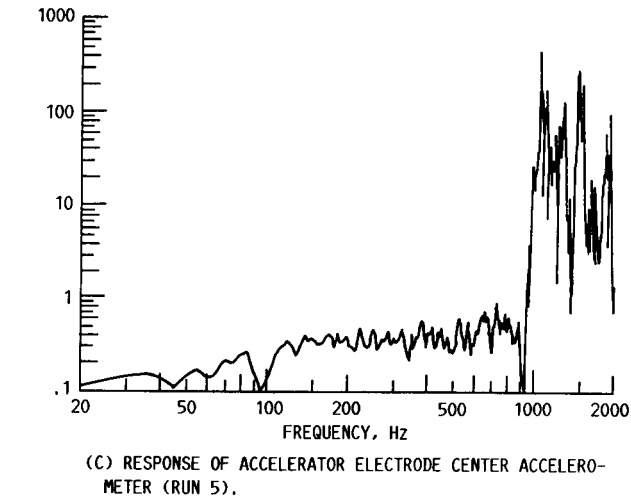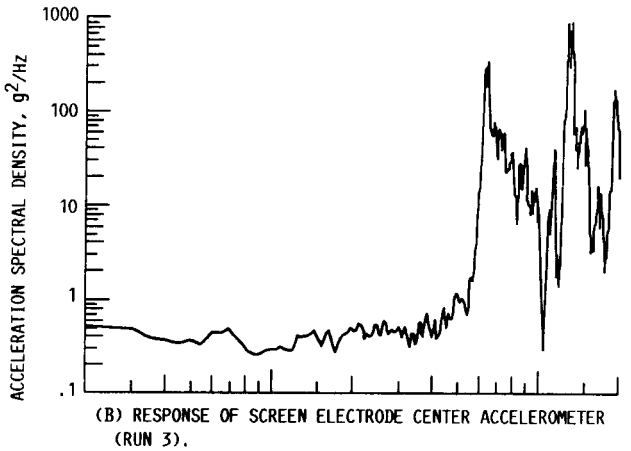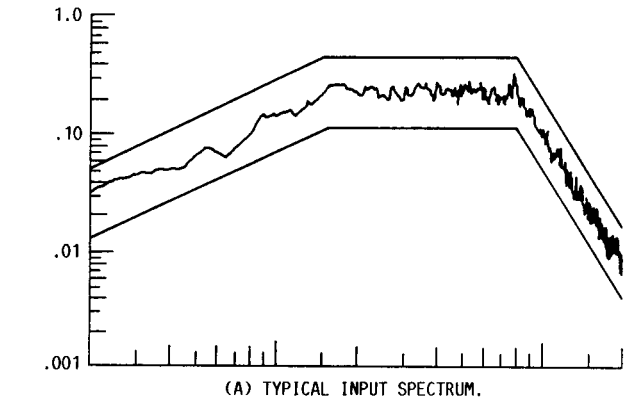LAUNCH VEHICLE, 4.2 g rms (RUN 2).

18

(A) TYPICAL INPUT SPECTRUM.

(B) RESPONSE OF SCREEN ELECTRODE CENTER ACCELEROMETER (RUN 3).

(C) RESPONSE OF ACCELERATOR ELECTRODE CENTER ACCELERO-METER (RUN 5).

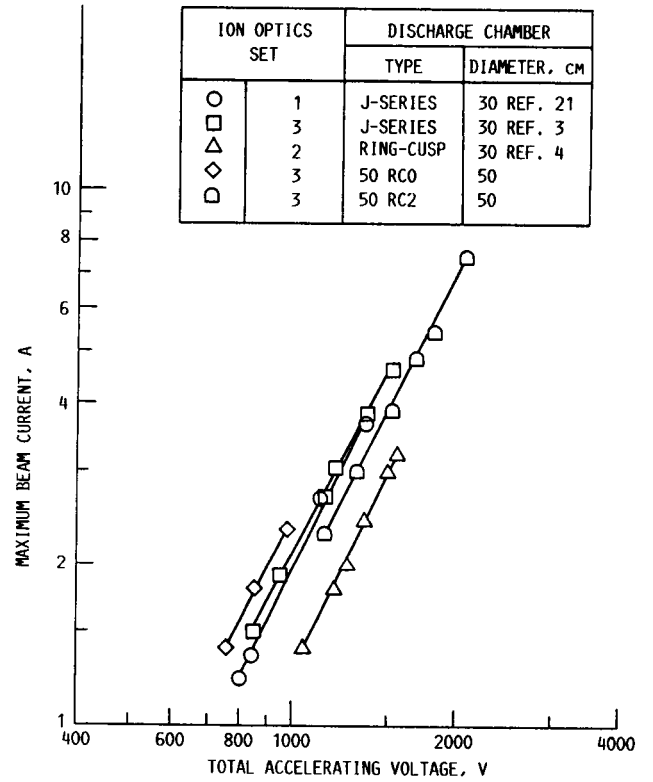FIGURE 9. - RANDOM VIBRATION, 15 g RMS (RUNS 3, 5, AND 6).



| ION OPTICS SET | | DISCHARGE CHAMBER | |
|---|---|---|---|
| | | TYPE | DIAMETER, CM |
| ○ | 1 | J-SERIES | 30 REF. 21 |
| □ | 3 | J-SERIES | 30 REF. 3 |
| △ | 2 | RING-CUSP | 30 REF. 4 |
| ◇ | 3 | 50 RCO | 50 |
| ⬭ | 3 | 50 RC2 | 50 |

FIGURE 10. - XENON ION EXTRACTION CAPABILITY OF 30-CM-DIAM ION OPTICS ON VARIOUS DISCHARGE CHAMBERS.
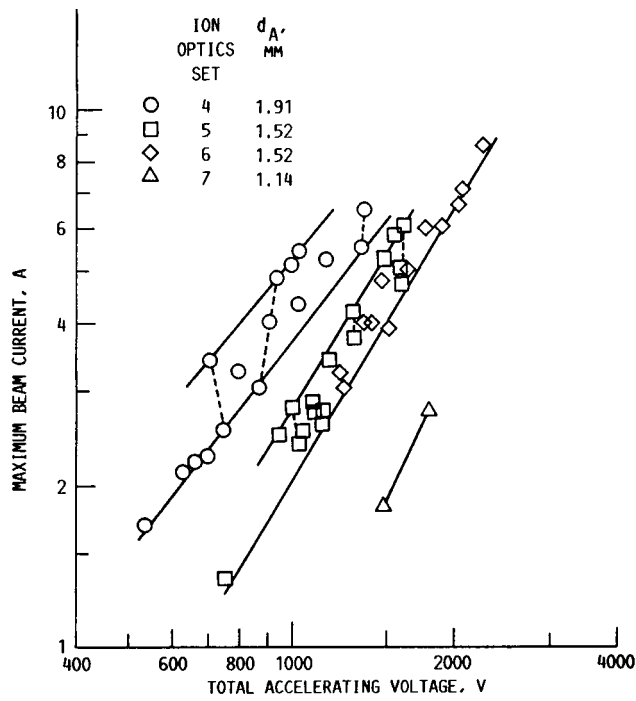
19

FIGURE 11. - ION EXTRACTION CAPABILITY OF 50-cm-diam ION OPTICS EVALUATED ON A DIVERGENT FIELD DISCHARGE CHAMBER.
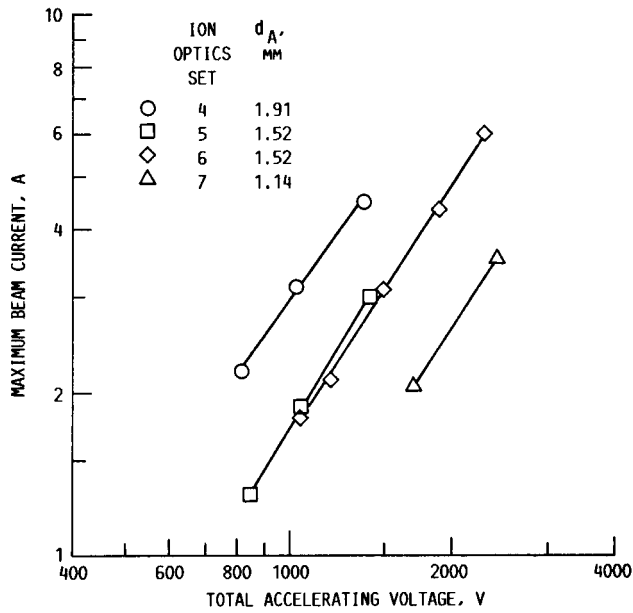


FIGURE 12. - ION EXTRACTION CAPABILITY OF 50-cm-diam OPTICS EVALUATED ON A RING-CUSP DISCHARGE CHAMBER.
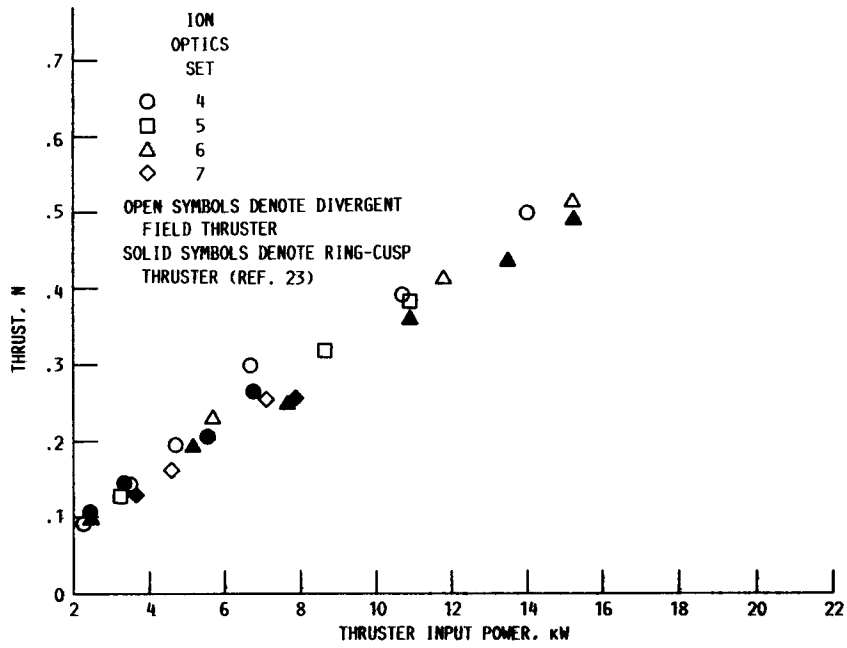
FIGURE 13. - THRUST AS A FUNCTION OF THRUSTER INPUT POWER FOR 50-CM-DIAM XENON ION THRUSTERS.
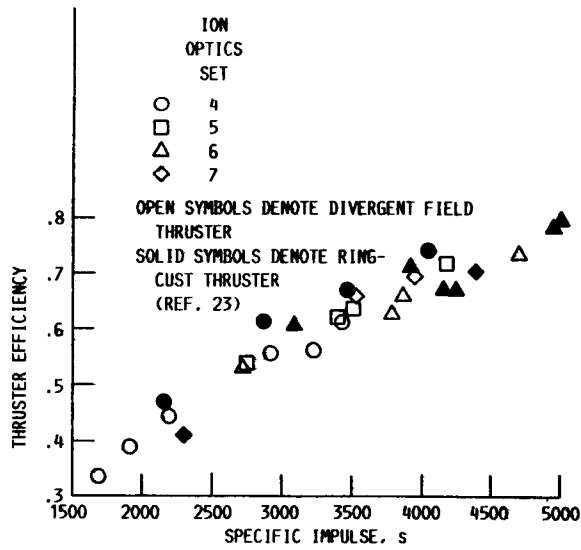


FIGURE 14. - THRUSTER EFFICIENCY AS A FUNCTION OF SPECIFIC IMPULSE FOR 50-CM-DIAM XENON ION THRUSTERS.

21

| | | |
|---|---|---|
| **NASA** National Aeronautics and Space Administration | Report Documentation Page | |

| 1. Report No. NASA TM-102143 AIAA-89-2717 | 2. Government Accession No. | 3. Recipient's Catalog No. |
|---|---|---|
| 4. Title and Subtitle<br><br>Ion Optics for High Power 50-cm-diam Ion Thrusters | | 5. Report Date<br>September 1989 |
| | | 6. Performing Organization Code |
| 7. Author(s)<br><br>Vincent K. Rawlin and Marc G. Millis | | 8. Performing Organization Report No.<br>E-4938 |
| | | 10. Work Unit No.<br>506-42-31 |
| 9. Performing Organization Name and Address<br><br>National Aeronautics and Space Administration<br>Lewis Research Center<br>Cleveland, Ohio 44135-3191 | | 11. Contract or Grant No. |
| 12. Sponsoring Agency Name and Address<br><br>National Aeronautics and Space Administration<br>Washington, D.C. 20546-0001 | | 13. Type of Report and Period Covered<br>Technical Memorandum |
| | | 14. Sponsoring Agency Code |

15. Supplementary Notes

16. Abstract

Propulsion systems analyses have indicated that high power xenon ion thrusters can enable the use of cost saving smaller launch vehicles for orbit transfer missions. Fifty-cm diameter thrusters, proposed to satisfy the mission requirements, have been fabricated and evaluated. Because the ion optics are considered to be the most critical component, they were subjected to extensive mechanical and electrical evaluation. The ion optics fabrication process, used at NASA Lewis Research Center for the past 18 years to make 30- and 50-cm diameter ion optics was described. Fifty-cm diameter ion optics were vibration tested with no apparent damage. The ion extraction capabilities of 30- and 50-cm diameter ion optics were evaluated on divergent field and ring-cusp discharge chambers and compared. Sensitivities of perveance to discharge chamber type, discharge chamber power, and accelerator electrode hole diameters were observed. Thrust and input power levels up to 0.64 and 20 kW, respectively, were demonstrated with the divergent field discharge chamber. Thruster efficiencies and specific impulse values up to 79 percent at 5000 sec were achieved.

| 17. Key Words (Suggested by Author(s))<br><br>Ion thrusters; Xenon ion; Ion propulsion;<br>Electric propulsion; Ion accelerators | 18. Distribution Statement<br><br>Unclassified – Unlimited<br>Subject Category 20 | | |
|---|---|---|---|
| 19. Security Classif. (of this report)<br>Unclassified | 20. Security Classif. (of this page)<br>Unclassified | 21. No of pages<br>22 | 22. Price*<br>A03 |